A combined isotropic, kinematic and distortional hardening model for aluminum and steels under complex strain-path changes

Jisheng Qin [a], Bjørn Holmedal [a] and Odd Sture Hopperstad [b,c]

[a] Department of Materials Science and Engineering, Norwegian University of Science and Technology (NTNU), NO-7491 Trondheim, Norway

[b] Department of Structural Engineering, NTNU, NO-7491 Trondheim

[c] Centre for Advanced Structural Analysis (CASA), NTNU, NO-7491 Trondheim

qin_jisheng@hotmail.com, bjorn.holmedal@ntnu.no, odd.hopperstad@ntnu.no

Corresponding author: Jisheng Qin

Abstract

In this work, a new model is proposed for predicting stress transients caused by strain path changes. The model is formulated in stress space, where a second order tensor, i.e., the microstructure stress deviator, is used to memorize and model the evolution history of the microstructure. Both its direction and magnitude are used to transiently distort the yield surface and to modify the work hardening. Orthogonal strain-path changes are handled by yield surface distortions, while Bauschinger effects are described by a kinematic hardening formulation. The model is calibrated to, and captures well, earlier published experiments for commercial pure aluminum, an extra deep drawing quality steel and a dual-phase steel. The proposed model describes qualitatively the response to double strain-path changes in low carbon steels. Efforts are made to design a relatively simple model as compared to the high complexity of the experiments, applying simple mathematical sub-models with straightforward interpretations and enabling a numerically stable implementation.

Keywords: A. Yield condition; B. Anisotropic material; B. Metallic material; B. Constitutive behavior; Strain-path change.

1. Introduction

Compared with proportional loading, strain-path changes (SPCs) induce transients of hardening or softening during the subsequent forming process. The most obvious influences are on springback and forming limits. In sheet metal forming processes, springback needs to be compensated (Boers et al., 2010; Lee et al., 2012). The forming limit curve (FLC) (Keeler and Backofen, 1963) is normally measured by proportional loading. However, the SPCs always exist and result in anisotropic hardening of the materials (Cao et al., 2000; Yao and Cao, 2002). Hence, a precise description of the material properties after complex SPCs is very important.

SPCs can be defined either in the strain rate space (Schmitt et al., 1994) or in the deviatoric stress space (Barlat et al., 2011). For abrupt SPCs, Barlat et al. (2011) proposed the measure

$$\cos\theta = \frac{\boldsymbol{\sigma}_1' : \boldsymbol{\sigma}_2'}{\|\boldsymbol{\sigma}_1'\|\|\boldsymbol{\sigma}_2'\|} \tag{1}$$

where $\boldsymbol{\sigma}_1'$ and $\boldsymbol{\sigma}_2'$ refer to the deviatoric stress tensors before and after the SPC, respectively, and $\|\mathbf{T}\| = \sqrt{T_{ij}T_{ij}}$ denotes the norm of the second order tensor $\mathbf{T}$. For cases of monotonic and reverse loading, $\cos\theta$ equals $+1$ and -1, respectively. Even though the original Schmitt angle (Schmitt et al., 1994) was formulated in the strain rate space, the angle θ is also referred to as the Schmitt angle. The term orthogonal deformation refers to $\cos\theta = 0$, i.e., the Schmitt angle θ is equal to 90°.

Examples of stress-strain curves of typical sheet metals subjected to reverse and orthogonal SPCs are sketched in Fig. 1. The phenomenon that the reloading yield stress is smaller than the unloading yield stress after a reverse SPC, is denoted the Bauschinger effect (Hasegawa et al., 1975; Bauschinger, 1881), as shown in Fig. 1a. The reloading hardening rate will often be much higher than the hardening rate under monotonic straining. For some materials, hardening stagnation will occur, i.e., a subsequent temporary decrease of the hardening rate. Commonly, transients induced by SPCs will vanish after a certain plastic strain, and the reloading stress-strain curve will coalesce with the monotonic loading curve (Ha et al., 2013). However, in some metals and alloys, permanent softening occurs, which means that the stress-strain curve is permanently affected by the reverse SPC. Eventually, the hardening rate may resume that of the monotonic curve, but the strength is still decreased permanently (Orowan et al., 1959; Li and

Bate, 1991). For a number of materials, orthogonal hardening (Ha et al., 2013; Mánik et al., 2015) or softening (Ha et al., 2013) transients take place after an orthogonal SPC, as shown in Fig. 1b. Permanent softening may also be observed after orthogonal SPCs (Mánik et al., 2015).

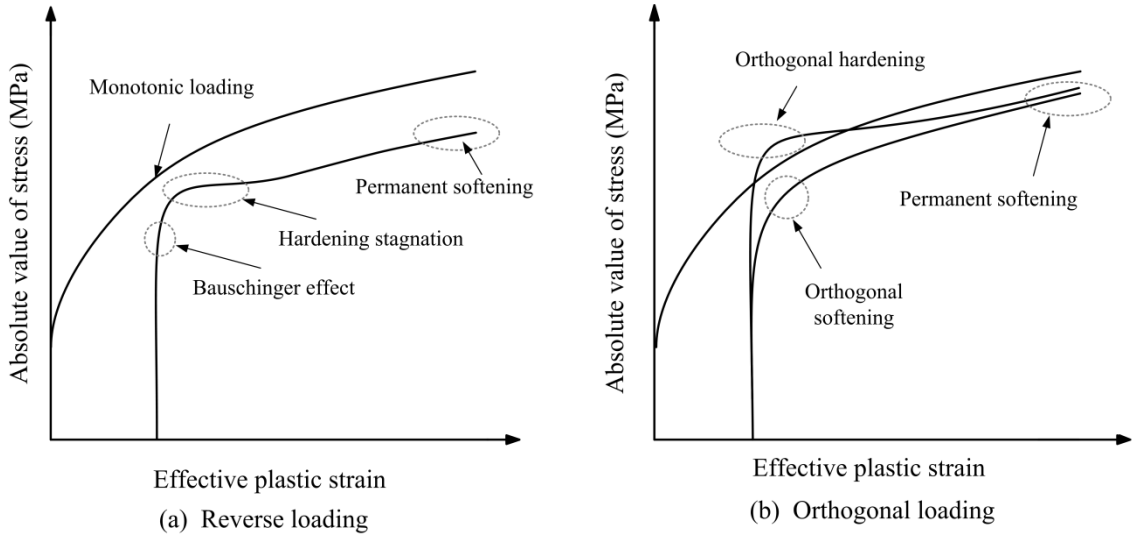

Fig. 1. The effect of different loading paths on the macroscopic material response for monotonic, reversed and orthogonal strain-paths

This paper considers phenomenological continuum plasticity models. A yield surface and an isotropic hardening rule are commonly used to describe the yielding and the hardening behavior of materials subjected to proportional loading (Barlat et al., 2003a; Yoshida et al., 2015). In order to capture the transients after SPCs, numerous models have been proposed, either using crystal plasticity formulations(Peeters et al., 2001a; Holmedal et al., 2008; Kitayama et al., 2013; Wen et al., 2015, 2016) or continuum plasticity (Haddadi et al., 2006; Wang et al., 2008; Barlat et al., 2013, 2014; Mánik et al., 2015). Basically, the continuum plasticity models can be divided into two groups as described in the following.

The first group modifies the flow stress by combined isotropic and kinematic hardening, while keeping the shape of the yield surface. This strategy was first proposed by Teodosiu and Hu (1995) and has been applied in many works (Bouvier et al., 2005; Wang et al., 2006, 2008). Choi et al. (2006) demonstrated a model which enables the anisotropic yield surface to expand, translate and rotate while the shape remains unchanged. Strategies for the numerical analysis and parameter identification were illustrated by Haddadi et al. (2006). The Teodosiu-Hu model applies second and forth orders tensors to predict transients, which do not affect permanently the

work hardening during subsequent monotonic loading. Mánik et al. (2015) proposed a model using only second order tensors to predict the SPC behavior. This model also accounts for changes of the work hardening during the SPC transients.

The other group of models distorts the yield surface. The distortion can be done either before the SPC (pre-distortion) or after the SPC (post-distortion). Hence, a specific phenomenological model can be classified as a pre-distortion model when the yield surface is distorted during preloading and as a post-distortion model when the yield surface is distorted after SPCs. Levkovitch and Svendsen (2007) proposed a pre-distortion model considering pressure dependence, which was motivated by polycrystalline modeling. Comparison of the Teodosiu-Hu model and the model proposed by Levkovitch and Svendsen (2007) was done by Boogaard and Riel (2009) and Clausmeyer et al. (2009). A directional pre-distortion hardening model within the framework of thermodynamics was proposed by Feigenbaum and Dafalias (2007).

In order to capture the Bauschinger effect by pre-distortion of the yield surface rather than translation by kinematic hardening, the homogeneous anisotropic hardening (HAH) yield criterion formalism for pre-distorting any isotropic or anisotropic yield surface was proposed by Barlat et al. (2011). The HAH pre-distortion model for reversal effects was complemented by an isotropic post-expansion of the yield surface to capture cross-hardening transients, in a framework with a dislocation-based work hardening model (Barlat et al., 2013; Ha et al., 2013). Another formulation but with distortional post-expansion of the yield surface in two in-plane directions relatively to the microstructure deviator, was suggested by He et al. (2013). Their model depends on a prescribed rotation angle defined in the plate plane, which in practice limits the model to plane stress deformation. A more general modification, the “enhanced HAH model”, was suggested by Barlat et al. (2014) and successfully applied to predict the orthogonal hardening behavior of an extra deep drawing quality (EDDQ) steel by post-distortion of the yield surface in its orthogonal directions, and to orthogonal softening behavior of a dual-phase steel by pre-distortion of the yield surface in its orthogonal directions. Furthermore, this model was able to qualitatively capture the measured behavior subsequent to double SPC transients of low carbon steel (Vincze et al., 2013). As discussed in Manopulo et al. (2015), the HAH model responds according to its anisotropic yield function in the case of proportional loading. This model has a complex mathematical formulation with a complex interpretation of how its

parameters are related to the experiments, but the model allows for a clear uncoupling of the Bauschinger parameters from the latent hardening coefficients. It is reported in Qin et al. (2017) that the HAH models have some challenges with respect to numerical convergence for purely orthogonal SPCs.

The transients after simple single SPCs of aluminum and steel have been captured well by several models (Peeters et al., 2001b; Haddadi et al., 2006; Levkovitch and Svendsen, 2007; Wang et al., 2008; Barlat et al., 2013, 2014; Mánik et al., 2015). However, so far, only the enhanced HAH model (Barlat et al., 2014) can capture, at least in a qualitatively correct manner, the transients occurring after double SPCs in low carbon steel. In Qin et al. (2017), the models proposed by Barlat et al. (2014) and Mánik et al. (2015) were compared and evaluated based on existing experimental data for commercially pure aluminum and EDDQ steel. The objective of the present paper is to propose a new distorted yield surface formulation, which can capture the features of both single and double SPCs and enable a robust numerical implementation. This will be an alternative to the enhanced HAH model. The modelling framework combines the simplicity of the model by Mánik et al. (2015) with a new formulation of orthogonal post-distortion of the yield surface, but unlike the HAH model, a kinematic hardening model captures load reversal effects.

2. Model formulation

The model formulation follows closely the ideas and formalism of Mánik et al. (2015), but the microstructure deviator is evolving in deviatoric stress space rather than in strain rate space, and during orthogonal hardening transients, the yield surface is distorting and expanding in its orthogonal directions in additional to its the original shape-invariant expansion. The formulation described here is restricted to small elastic strains as well as isothermal and rate-independent conditions.

A corotational formulation based on hypoelastic-plasticity theory is applied (Khan and Huang, 1995). All the tensorial quantities are expressed in the corotational frame. The transformations of the Cauchy stress tensor $\boldsymbol{\sigma}$ and the rate-of-deformation tensor $\mathbf{D}$ between the fixed and corotational coordinate systems are given by

$$\hat{\boldsymbol{\sigma}} = \mathbf{R}^T \boldsymbol{\sigma} \mathbf{R}, \quad \hat{\mathbf{D}} = \mathbf{R}^T \mathbf{D} \mathbf{R} \tag{2}$$

where $\hat{\boldsymbol{\sigma}}$ and $\hat{\mathbf{D}}$ are the corotational Cauchy stress tensor and corotational rate-of-deformation tensor, respectively, and $\mathbf{R}$ is the rotation tensor here defined by the polar decomposition of the deformation gradient (Belytschko et al., 2013).

The corotational rate-of-deformation $\hat{\mathbf{D}}$ can be additively decomposed into elastic and plastic parts

$$\hat{\mathbf{D}} = \hat{\mathbf{D}}^e + \hat{\mathbf{D}}^p \tag{3}$$

where $\hat{\mathbf{D}}^e$ and $\hat{\mathbf{D}}^p$ are the elastic and plastic corotational rate-of-deformation tensors, respectively. The relation between the corotational stress rate tensor and the elastic corotational rate-of-deformation tensor is written as

$$\frac{D\hat{\boldsymbol{\sigma}}}{Dt} = \hat{\mathbf{C}} : \hat{\mathbf{D}}^e = \hat{\mathbf{C}} : \left(\hat{\mathbf{D}} - \hat{\mathbf{D}}^p \right) \tag{4}$$

where $\hat{\mathbf{C}}$ is the fourth-order tensor of elastic moduli. In the corotational formulation, $\hat{\mathbf{C}}$ can be anisotropic but elastic isotropy is assumed here, and $\hat{\mathbf{C}}$ is defined by Young's modulus E and Poisson's ratio ν. The plastic rate-of-deformation tensor is defined by the associated flow rule

$$\hat{\mathbf{D}}^p = \dot{\lambda} \frac{\partial \phi}{\partial \hat{\mathbf{S}}} \tag{5}$$

where $\dot{\lambda} \geq 0$ is the plastic multiplier, ϕ is a first-order homogeneous yield function defined in the following section, $\hat{\mathbf{S}} = \hat{\boldsymbol{\sigma}} - \hat{\mathbf{X}}$ is the overstress tensor, and $\hat{\mathbf{X}}$ is the backstress tensor.

2.1. The yield function

A first-order homogeneous yield function combined with isotropic hardening is suitable for describing the stress-strain behavior under monotonic loading. However, under non-proportional loading sequences, translation and distortion of the yield surface is required to describe both the Bauschinger effect and the orthogonal hardening effects. Thus, the yield criterion is given by

$$f(\hat{\mathbf{S}}') \equiv \phi(\hat{\mathbf{S}}') - \sigma_Y = 0 \tag{6}$$

where $\hat{\mathbf{S}}'$ is the deviatoric overstress tensor and $\sigma_Y = R + S_r$ is the yield stress. The initial yield stress and isotropic work hardening are represented by R, while S_r is the extra isotropic

expansion or shrinkage of the yield surface occurring after reverse SPCs. The yield function $\phi(\hat{\mathbf{S}}')$, i.e., the equivalent stress with respect to the backstress, is here defined on the form

$$\phi(\hat{\mathbf{S}}')=\left(g_1^q\varphi^q(\hat{\mathbf{S}}')+\frac{\left(\frac{3}{8}\right)^{\frac{q}{2}} g_2^q}{\left\|\hat{\mathbf{P}}\right\|^q}\left(\left|\hat{\mathbf{P}}:\hat{\mathbf{S}}'-\left|\hat{\mathbf{P}}:\hat{\mathbf{S}}'\right|\right\|^q+\left|\hat{\mathbf{P}}:\hat{\mathbf{S}}'+\left|\hat{\mathbf{P}}:\hat{\mathbf{S}}'\right|\right\|^q\right)\right)^{\frac{1}{q}} \tag{7}$$

where g_1 and g_2 are functions, as specified below, q is a parameter, and $\hat{\mathbf{P}}$ is the microstructure deviator that introduces a fading memory of the deformation history. The magnitude and direction of $\hat{\mathbf{P}}$ are associated with the density and orientation of the dislocation microstructure, but cannot be directly linked to the microstructure evolution. For a well-annealed material, the magnitude of $\hat{\mathbf{P}}$ equals zero. Any first-order positive homogenous isotropic or anisotropic yield function can be used as the stable component φ. The yield function ϕ is convex as long as φ is convex, according to the theory of convex analysis of positive homogeneous functions (Rockafellar, 1970; Barlat et al., 2011).

The two functions g_1 and g_2 are defined as follows

$$g_1^q=\left(\frac{R}{R+S_o\left\|\hat{\mathbf{P}}\right\|}\right)^q, \quad g_2^q=1-g_1^q \tag{8}$$

where $S_o\left\|\hat{\mathbf{P}}\right\|$ captures the extra hardening transients after orthogonal SPCs. The evolution equation for the variable S_o is given in Section 2.4. According to Equations (7) and (8), the yield function ϕ equals the stable component φ when S_o equals zero, and thus the fluctuating component of the yield function is only used to describe cross-hardening effects due to orthogonal SPCs. Note that in Equation (7) the factor $\left\|\hat{\mathbf{P}}\right\|^{-q}$ never creates a singularity, since $\phi\left(\hat{\mathbf{P}}\to\mathbf{0}\right)=\varphi$, due to that $\lim_{\hat{\mathbf{P}}\to 0} g_1=1$.

The evolution of $\hat{\mathbf{P}}$ is defined in the deviatoric stress space according to

$$\dot{\hat{\mathbf{P}}}=\hat{\mathbf{h}}_P\dot{\lambda}, \quad \hat{\mathbf{h}}_P=\frac{1}{k_P\Delta\varepsilon_P}\left(k_P\hat{\mathbf{N}}-\hat{\mathbf{P}}\right), \quad \hat{\mathbf{N}}=\frac{\hat{\mathbf{S}}'}{\left\|\hat{\mathbf{S}}'\right\|} \tag{9}$$

where $\hat{\mathbf{N}}$ is the normalized deviatoric overstress tensor. In Equation (9), $k_p\hat{\mathbf{N}}$ acts as an attractor for the microstructure deviator, while $k_p\Delta\varepsilon_P$ controls the strain scale of the saturation of $\hat{\mathbf{P}}$. The parameter $k_p \in [0,1]$ is defined by

$$k_P = \begin{cases} (1-\alpha)+\alpha\cos\theta & \text{if} \quad \hat{\mathbf{P}}:\hat{\mathbf{S}}' \geq 0 \\ (1-\alpha)+\alpha\cos^4\theta & \text{if} \quad \hat{\mathbf{P}}:\hat{\mathbf{S}}' < 0 \end{cases} \tag{10}$$

where $\alpha \in [0,1]$ is a constant, and the Schmitt angle θ is here defined as

$$\cos\theta = \frac{\hat{\mathbf{S}}':\hat{\mathbf{P}}}{\|\hat{\mathbf{S}}'\|\|\hat{\mathbf{P}}\|} = \frac{\hat{\mathbf{N}}:\hat{\mathbf{P}}}{\|\hat{\mathbf{P}}\|} \tag{11}$$

The $\cos^4\theta$ term for $\hat{\mathbf{P}}:\hat{\mathbf{S}}' < 0$ is introduced to retain a small value of k_P during the first part of the transient. A physical argument for the asymmetry of k_P is that elements of the old dislocation microstructures will first have to be erased after a SPC with a reversal component (Barlat et al., 2003b), i.e., k_P remains small when $\hat{\mathbf{P}}:\hat{\mathbf{S}}' < 0$. However, as $\hat{\mathbf{P}}$ rotates towards $\hat{\mathbf{N}}$ and the scalar product $\hat{\mathbf{P}}:\hat{\mathbf{S}}'$ becomes positive, new microstructure will gradually be built, corresponding to a larger value of k_P.

2.2. Isotropic hardening

Isotropic hardening implies shape-preserving expansion of the elastic region in the deviatoric stress space during plastic deformation governed by the hardening variables R and S_r .

The evolution equation for the hardening variable R is defined by

$$\dot{R} = \sum_{i=1}^{2}\dot{R}_i + \left(h_r^{tr} + h_o^{tr}\right)\dot{\lambda} \tag{12}$$

where R_1 and R_2 describe monotonic hardening. The effects of SPCs involving reverse and orthogonal loading on the hardening rate are defined by the softening moduli h_r^{tr} and h_o^{tr}, respectively. The evolution of R_1 and R_2 are here defined by a generalized Voce rule (Voce, 1948)

$$\dot{R}_i = h_{R_i}\dot{\lambda}, \quad h_{R_i} = \frac{R_i^{sat} - R_i}{\Delta\varepsilon_{R_i}}, \quad i = 1,2 \tag{13}$$

where R_i^{sat} gives the saturation value of hardening term R_i, and $\Delta\varepsilon_{R_i}$ controls its strain scale for its saturation. The analytical solutions of these evolution equations are

$$R_i(\bar{\varepsilon}) = R_i^{sat}\left(1 - \exp\left(-\frac{\bar{\varepsilon}}{\Delta\varepsilon_{R_i}}\right)\right), \quad i = 1,2 \tag{13}$$

where the equivalent plastic strain is defined by $\bar{\varepsilon} = \int_0^t \dot{\lambda} dt$. The initial values of R_1 and R_2 are zero, while the initial value of R is the initial yield stress R_0.

The two softening moduli h_r^{tr} and h_o^{tr} are introduced to capture the permanent softening behavior after reverse and orthogonal SPCs, respectively. The softening modulus h_r^{tr} reduces the work hardening rate during the transient occurring subsequent to a reverse SPC and thus leads to permanent softening

$$h_r^{tr} = k_r \min\left(\|\hat{\mathbf{P}}\|\cos\theta, 0\right) \tag{14}$$

where k_r controls the magnitude of the deviation between the reverse loading curve and the monotonic loading curve. The above formulation implies that when reverse loading happens, the permanent softening term will be activated. Similarly, the softening modulus h_o^{tr} modifies the work hardening rate after orthogonal SPCs and also causes permanent softening

$$h_o^{tr} = -k_o \|\hat{\mathbf{P}}\|\sin\theta \tag{15}$$

The parameter k_o reflects the magnitude of the deviation between the reloading loading curve after orthogonal SPC and the monotonic loading curve.

Kinematic hardening can describe the Bauschinger effect, but cannot capture hardening stagnation, i.e., the inflection point on the stress-strain curve after reverse loading. This reverse behavior is here modeled by a combination of kinematic hardening and transient isotropic hardening. The evolution of the transient hardening variable S_r is given by

$$\dot{S}_r = h_{S_r}\dot{\lambda}, \quad h_{S_r} = \frac{-S_r^{sat}\min\left(\|\hat{\mathbf{P}}\|\cos\theta, 0\right) - S_r}{\Delta\varepsilon_r}, \quad S_r^{sat} = q_r R \tag{16}$$

The constant q_r relates the saturation of the strength transient to the hardening variable R. The parameter $\Delta\varepsilon_r$ controls the strain scale of this saturation process. The initial value of S_r is set to zero. After the reverse SPC, implying that $\hat{\mathbf{S}}'$ is temporarily in the opposite direction of $\hat{\mathbf{P}}$, S_r rapidly increases and saturates towards $-S_r^{sat}\|\hat{\mathbf{P}}\|\cos\theta$, and then decreases to zero as the microstructure deviator $\hat{\mathbf{P}}$ rotates towards the current loading direction as defined by the unit tensor $\hat{\mathbf{N}}$.

2.3. Kinematic hardening

The deviatoric backstress tensor $\hat{\mathbf{X}}$, which defines the center of the elastic region in deviatoric stress space, is used to describe the kinematic hardening. The nonlinear hardening rule of Armstrong and Frederick (1966) is used to describe the evolution of the backstress tensor, viz.

$$\hat{\mathbf{X}} = \sum_{i=1}^{2}\hat{\mathbf{X}}_i, \quad \dot{\hat{\mathbf{X}}}_i = \hat{\mathbf{h}}_{X_i}\dot{\lambda}, \quad \hat{\mathbf{h}}_{X_i} = \frac{1}{\Delta\varepsilon_{X_i}}\left(X_i^{sat}\frac{\hat{\mathbf{S}}'}{\phi(\hat{\mathbf{S}}')} - \hat{\mathbf{X}}_i\right) \tag{17}$$

where $\hat{\mathbf{X}}_i$ are the partial backstress tensors. The parameter X_i^{sat} represents the saturation value of $\hat{\mathbf{X}}_i$, while $\Delta\varepsilon_{X_i}$ defines the strain scale of the saturation processes. The initial values of the backstress tensors are $\hat{\mathbf{X}}_i(0) = \mathbf{0}$.

Note that the use of kinematic hardening also leads to a drop of the yield stress after an orthogonal SPC, caused by the shift of the yield surface during deformation prior to the SPC.

2.4. Distortional hardening

The extra strength subsequent to orthogonal SPCs is here modeled by the scalar variable S_o, which distorts the yield surface by expanding it in stress directions orthogonal to $\hat{\mathbf{P}}$. The evolution of S_o is defined by

$$\dot{S}_o = h_{S_0}\dot{\lambda}, \quad h_{S_o} = \frac{S_o^{sat}\sin^n\theta - S_o}{\Delta\varepsilon_o}, \quad S_o^{sat} = q_o R \tag{18}$$

where $0 \le \theta \le \pi$ so that $0 \le \sin\theta \le 1$. It is worth noting that even though S_o plays a similar role as in Mánik et al. (2015), the mathematical formulation here is different, the main difference being that it is here applied to expand the yield surface only in orthogonal directions, as compared to the isotropic expansion in the MHH model. The constant q_o relates the saturation of the strength transient to the isotropic hardening R, and $\Delta\varepsilon_o$ controls the strains scale of the saturation processes. The initial value of S_o is zero. Subsequent to the SPC, S_o rapidly increases and saturates towards $S_o^{sat}\sin^n\theta$, and then, according to Equation (11), decreases to zero as the microstructure deviator $\hat{\mathbf{P}}$ rotates towards the current loading state $\hat{\mathbf{N}}$. The parameter n is used to describe the correct evolution of the stress overshoot subsequent to orthogonal SPCs along different angles. A positive value smaller or larger than unity will increase or decrease the strain range of the stress overshoot ratio, respectively.

During monotonic and reverse loading, S_o remains equal to zero, and, according to Equation (8), $g_1^q = 1$ and $g_2^q = 0$. By Equation (7), the yield criterion then becomes $f \equiv \varphi(\hat{\mathbf{S}}) - \sigma_Y = 0$, and it follows that during monotonic and reverse loading, yielding is described by the stable component φ of the yield function ϕ. Right after a purely orthogonal SPC, the scalar product $\hat{\mathbf{P}} : \hat{\mathbf{S}}'$ and the transient hardening variable S_r are equal to zero, and the yield criterion then becomes

$$f \equiv \phi(\hat{\mathbf{S}}') - R = \frac{R}{R + S_o\left\|\hat{\mathbf{P}}\right\|}\varphi\left(\hat{\mathbf{S}}'\right) - R = 0 \tag{19}$$

The equivalent stress $\phi(\hat{\mathbf{S}}')$ is equal to R and does not change abruptly after SPCs. However, the value of $\varphi\left(\hat{\mathbf{S}}'\right)$ is instantaneously equal to $R + S_o\left\|\hat{\mathbf{P}}\right\|$ and the subsequent orthogonal hardening behavior can be described by the stress overshoot $S_o\left\|\hat{\mathbf{P}}\right\|$ as S_o now rapidly increases. Note that the Bauschinger effect also influences the orthogonal SPCs because the back stress shifts the yield surface in stress space.

3. Parameter identification

There are 19 coefficients in the constitutive model in addition to the parameters of the stable component of the yield surface. In the following, the identification procedure is described in general terms, assuming that monotonic, reverse and orthogonal loading curves from experiments are available. Any homogeneous yield function describing the initial anisotropy of the material can be used as the stable component of the yield surface. The high-exponent, isotropic Hershey yield function was adopted for commercial pure aluminum by Mánik et al. (2015), while the high-exponent, anisotropic Yld2000-2d yield function was used for EDDQ and DP780 by Ha et al. (2013). The exponent m of the high-exponent yield functions was set to 8 for aluminum and 6 for steel (Barlat et al., 2003b).

The identification procedure consists of three steps that are repeated iteratively until converged values of the model coefficients are obtained. The procedure is as follows.

In the first step, the initial yield stress R_0 is determined and the isotropic hardening parameters (R_1^{sat}, $\Delta\varepsilon_{R_1}$, R_2^{sat}, $\Delta\varepsilon_{R_2}$) and the kinematic hardening parameters (X_1^{sat}, $\Delta\varepsilon_{X_1}$, X_2^{sat}, $\Delta\varepsilon_{X_2}$) are estimated from the monotonic and reverse loading curves without accounting for transients and permanent softening due to the SPC. In Fig. 2a, the drop of the yield stress after reverse loading, which is denoted $2X$, equals two times the back stress at the specific plastic prestrain. The reloading curves resulting from this first estimate of the parameters are illustrated with dashed lines in Fig. 2. Note that two terms may be used to describe the evolution of isotropic and kinematic hardening. However, they are not necessary if an acceptable description of the hardening behavior can be predicted with only one term, as is the case here.

In the second step, the strain scale $\Delta\varepsilon_P$ of the transient phase after reverse SPC is estimated, which determines the response of the microstructure deviator $\hat{\mathbf{P}}$, see Fig. 2a. The permanent softening, which is represented by the difference between the monotonic loading curve and the reloading curve after that the transient behavior has faded away, see Fig. 2a, is used to estimate the parameter k_r. Then, the parameters $\Delta\varepsilon_r$ and q_r that control the transient behavior during reverse SPC by the evolution of the internal variable S_r, are estimated. Their influence on the stress-strain transient is illustrated by the shaded area in Fig. 2a.

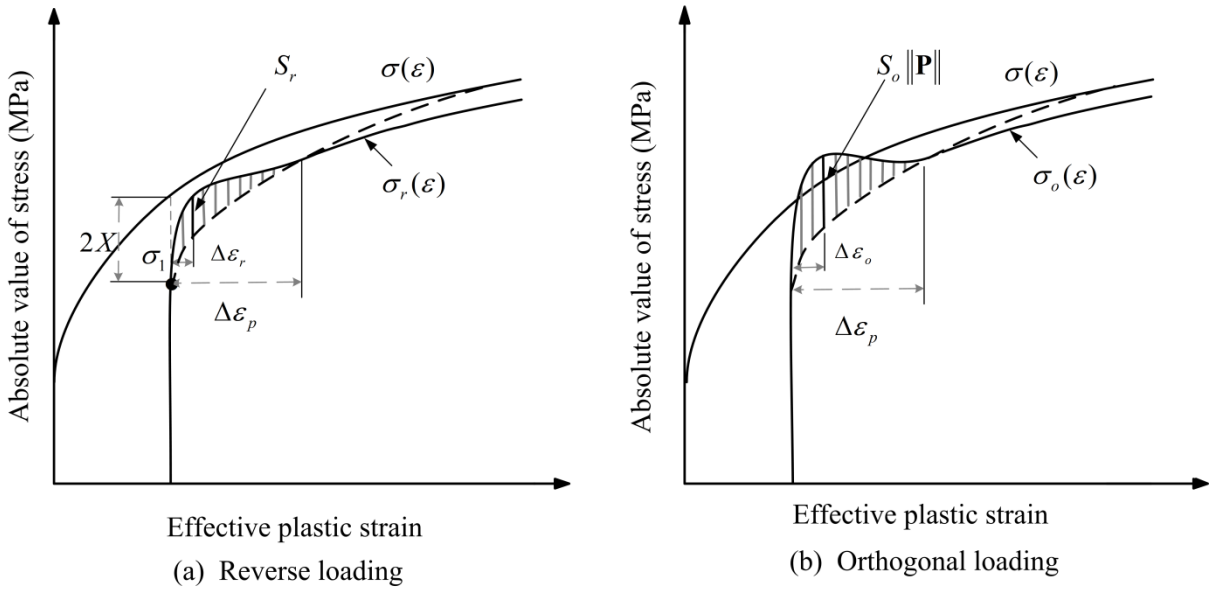

Fig. 2. Sketches of the loading curves and quantities used in the parameter identification process. The monotonic loading curve $\sigma = \sigma(\varepsilon)$ and the reloading curve after reverse and orthogonal SPCs, $\sigma = \sigma_r(\varepsilon)$ and $\sigma = \sigma_o(\varepsilon)$, respectively, are plotted with solid lines, while the reloading curve without transients and permanents softening due to SPCs is shown with dashed lines.

In the third step, the parameter k_o that reflects the permanent softening behavior after orthogonal loading, is first estimated by considering the difference between the monotonic loading curve and the reloading curve after an orthogonal SPC, see Fig. 2b. Then, the parameters $\Delta\varepsilon_o$ and q_o that govern the transient behavior during orthogonal SPC by the evolution of the internal variable S_o, are assessed, as illustrated by the shaded area in Fig. 2b. Finally, the parameters α and n are estimated by considering the stress overshoot of reloading curves with different angles after orthogonal SPCs.

In each step of the identification process, a first approximation was obtained iteratively by using a least squares method with a weighted sum of the differences between available experimental data and corresponding simulation results. It is worth noting that the inflection area should be given larger weights. Subsequently, a manual trial-and-error method was used to improve the calibration in each step. The sequence of steps was repeated several times to improve the calibration further.

4. Applications

Experimental results, including single SPCs of various kinds, have earlier been reported for commercially pure aluminum (AA1050), EDDQ and DP780 steels (Ha et al., 2013; Barlat et al., 2014; Mánik et al., 2015). In the following, the proposed constitutive model will be used to describe the behavior of these materials after complex single and double SPCs. The model constants obtained by using the parameter identification procedure outlined in the previous section, are listed in Table 1.

The use of two back stress tensors was justified in Mánik et al. (2015) in order to obtain the r-value transient of commercially pure aluminum. However, the current model cannot capure the r-value transient correctly even with two terms, hence only one kinematic hardening term was used for AA1050. The inflection point of the stress-strain curve occuring subsequent to the reverse SPC, could then be modelled entirely by the reduced work hardening rate during this transient, i.e., with the transient stress contribution S_r set to zero.

Owing to the lack of reversal tests for EDDQ steel and the experimental observation that this material does not exhibit permanent softening after orthogonal SPCs, the functions $\mathbf{X}_1$, $\mathbf{X}_2$ S_r, h_r^{tr} and h_o^{tr} were not employed for this material.

For the DP780 steel, the reported experiments indicate that this material does not exhibit orthogonal hardening and permanent softening after orthogonal SPC; hence, S_o and h_o^{tr} were not employed. The transient behavior of the reversal tests was also turned off, i.e., S_r and h_r^{tr} were not applied. Furthermore, only one kinematic hardening term was applied for this material.

The Hershey yield function (Hershey, 1954) was used for commercial pure aluminum, while the anisotropic Yld2000-2d yield function (Barlat et al., 2003a) was used for the two steels. The anisotropy coefficients of the Yld2000-2d yield function were taken from Ha et al. (2013).

Table 1 Model constants for commercially pure aluminum (CP-Al), EDDQ and DP780 steels

	q	R_0	R_1^{sat}	$\Delta\varepsilon_{R_1}$	R_2^{sat}	$\Delta\varepsilon_{R_2}$	X_1^{sat}	$\Delta\varepsilon_{X_1}$	X_2^{sat}	$\Delta\varepsilon_{X_2}$
	[–]	[MPa]	[MPa]	[–]	[MPa]	[–]	[MPa]	[–]	[MPa]	[–]
CP-Al	2	7	80	0.330	32	0.0230	7	0.0010	0	–
EDDQ	2	150	323	0.500	97	0.0400	0	–	0	–
DP780	2	471	385	0.108	52	0.0074	180.5	0.0074	0	–
	$\Delta\varepsilon_P$	α	q_0	$\Delta\varepsilon_o$	n	q_r	$\Delta\varepsilon_r$	k_0	k_r	
	[–]	[–]	[–]	[–]	[–]	[–]	[–]	[MPa]	[MPa]	
CP-Al	0.1	0.8	0.16	0.0004	0.25	0	–	100	1300	
EDDQ	0.2	0.8	0.38	0.0010	0.25	0	–	0	0	
DP780	–	0	0	–	0	0	–	0	0	

4.1. Single SPCs of commercially pure aluminum

Mánik et al. (2015) studied the stress-strain behavior of initially isotropic, commercially pure aluminum after reverse and orthogonal SPCs. Abrupt SPCs were obtained by performing tension tests in various directions subsequent to prestraining by compression or rolling. In Fig. 3, the simulated stress-strain curves after reverse SPCs are compared with the experimental data. The proposed model captures the Bauschinger effect, the hardening stagnation and the permanent softening after reverse SPCs. The initial yield stress of the reverse loading curve for 4.4% prestrain is slightly higher than the experimental data.

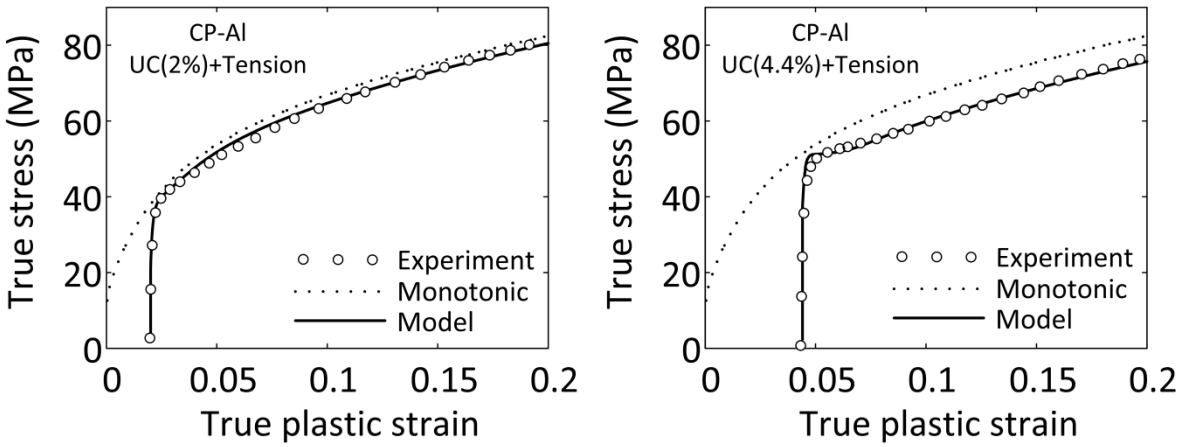

Fig. 3. Commercially pure aluminum: Experimental and simulated stress–strain curves in uniaxial tension after prestraining by uniaxial compression (2% and 4.4%), together with the monotonic loading curve.

The experimental and simulated behaviors of commercially pure aluminum in uniaxial tension along various loading directions after prestraining to different levels by rolling are shown in Fig. 4. For a given prestrain, the reloading curve reaches almost instantaneously a higher value than the monotonic loading curve. Then, permanent softening occurs with further straining. Finally, the hardening rate of the reloading loading curve approaches that of the monotonic loading curve. The permanent softening results in a lower flow stress. The model captures with good accuracy both the stress overshoot and the permanent softening observed experimentally.

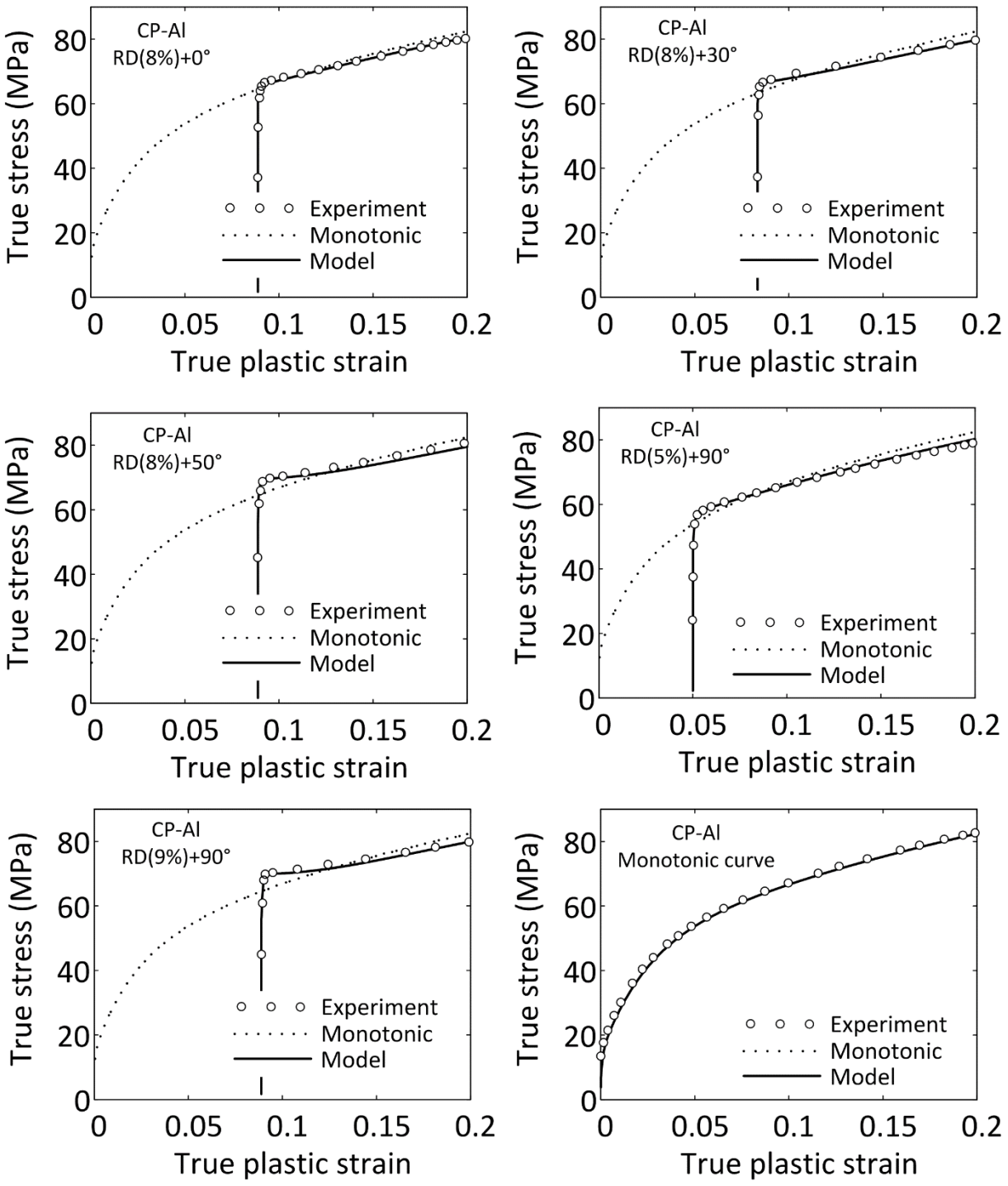

Fig. 4. Commercially pure aluminum: Experimental and simulated stress–strain curves in uniaxial tension along various directions after prestraining by rolling, together with the monotonic loading curve.

4.2. Single and double SPCs of EDDQ steel

Ha et al. (2013) reported tests on an EDDQ steel, i.e., a low carbon steel with high r-values. Uniaxial tensile tests were performed at every 15° from the rolling direction after prestraining to 4% and 10% in uniaxial tension along the rolling direction. Large samples were prestrained, from which small samples subsequently were cut at different angles.

The experimental and simulated monotonic loading curves in the rolling direction (0°) are shown in Fig. 5. Also the simulated monotonic loading curves in the other orientations compare well with the experimental counterparts.

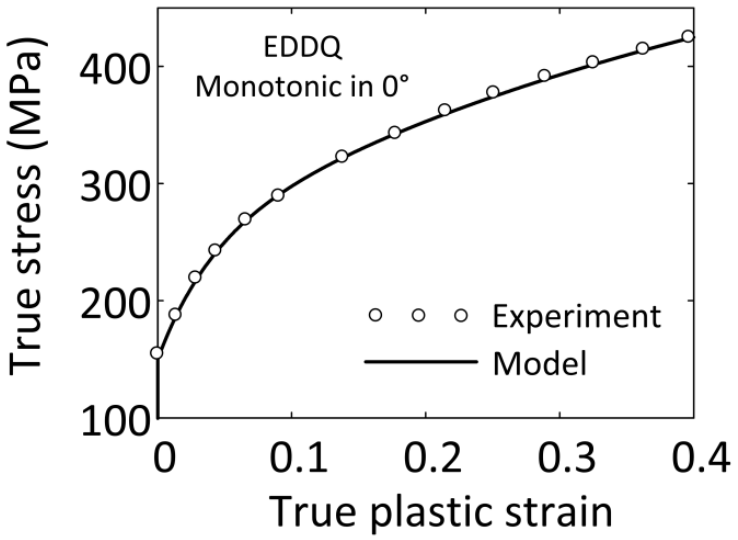

Fig. 5. EDDQ steel: Experimental and simulated monotonic loading curve in uniaxial tension along the rolling direction (0°).

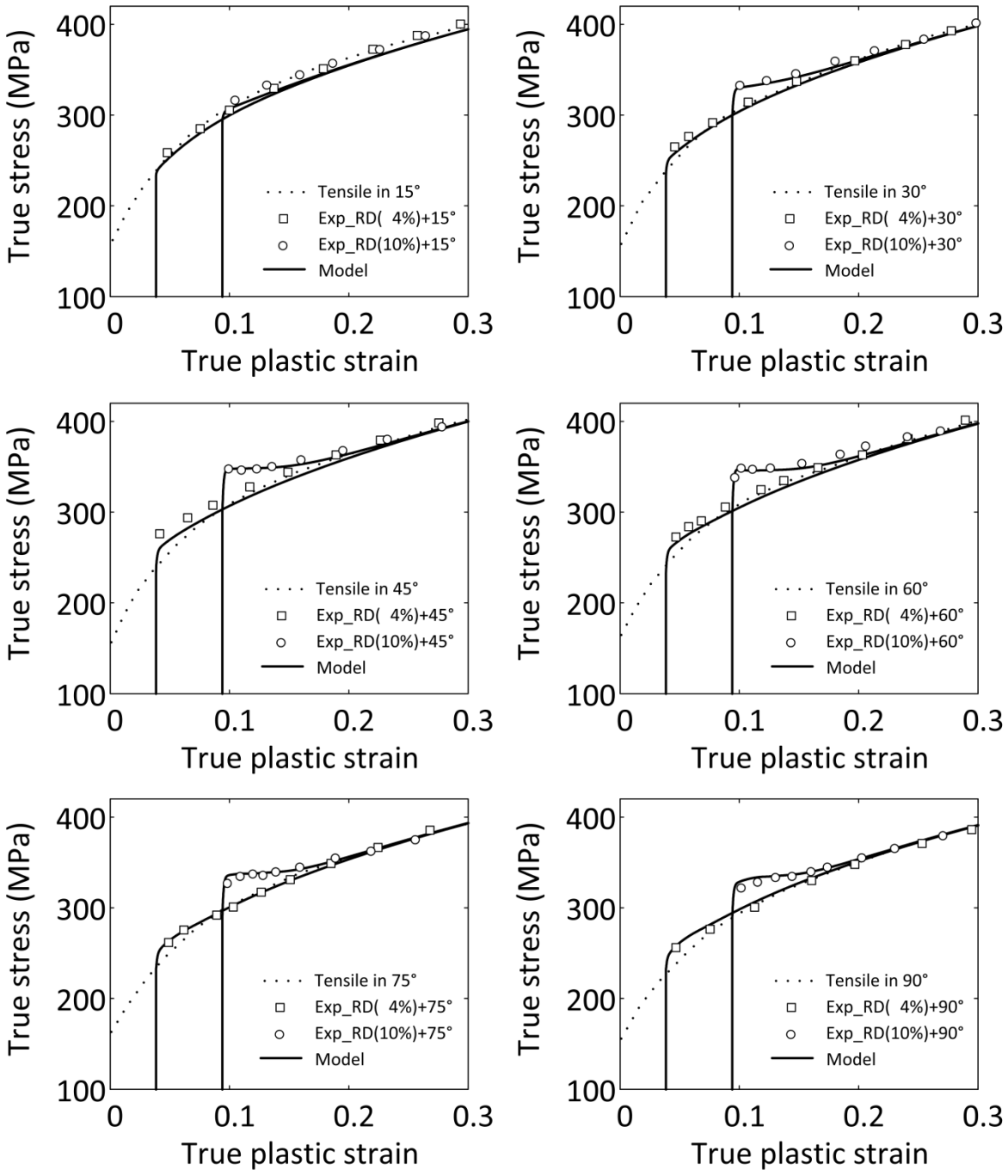

Fig. 6. EDDQ steel: Experimental and simulated reloading curves in tension at every 15° after 4% and 10% prestrain in tension along the rolling direction, together with the monotonic loading curve in the reloading direction.

The experimental and simulated reloading curves for every 15° after 4% and 10% prestraining are presented in Fig. 6. Extra hardening transients occur after orthogonal SPCs. The stress overshoot and the duration of the transients increase with increased prestraining. The maximum stress overshoot is obtained along the 45° orientation. The model captures the stress overshoot of all reloading curves with prestrain of 10% as well as the duration of the transient behavior. However, the predicted yield stresses of the reloading curves with prestrain of 4% along the 45° and 60° orientations are slightly lower than the experimental data. The behavior in the other orientations after 4% prestrain is well described.

The proposed constitutive model was also applied to predict the behavior of EDDQ steel after double SPCs consisting of 6% tensile prestraining in the rolling direction (RD), followed by 2%, 5% or 10% tensile straining in the 45° orientation and finally reloading in tension along the RD. The behavior of low carbon steel after double SPCs has been experimentally investigated by Vincze et al. (2013) and the EDDQ steel is expected to exhibit a similar behavior. Fig. 7 shows the simulated stress-strain curves after the double SPCs obtained with the QHH model as well as the enhanced HAH model (Barlat et al., 2014). The parameters of the enhanced HAH model were taken from Qin et al. (2017). The results of both models are in qualitative agreement with the experimental results of Vincze et al. (2013). In particular, the different strain scale of the transient in the third loading curve compared with the second loading curve is notable.

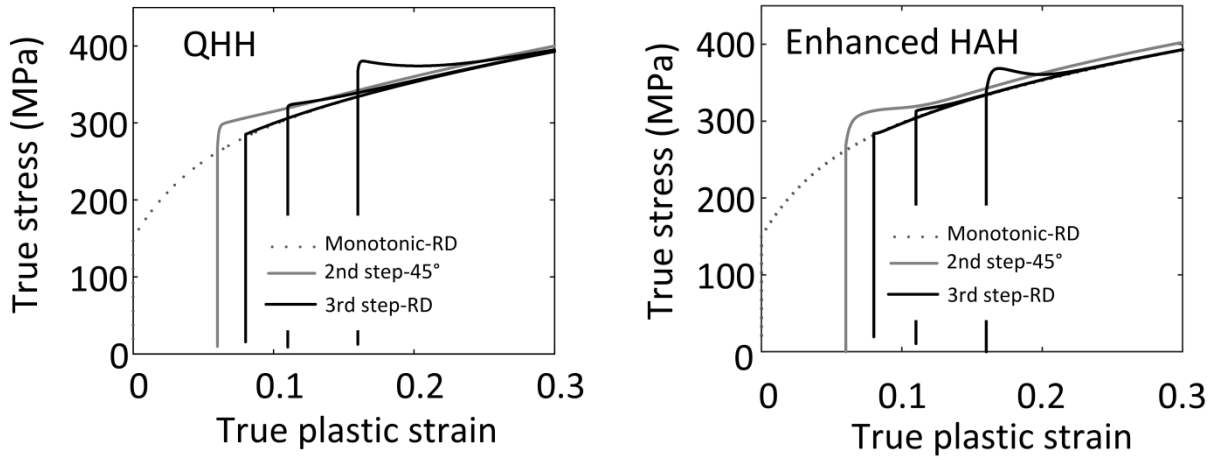

Fig. 7. EDDQ steel: Simulated double SPCs with the QHH model and the enhanced HAH model consisting of 6% tensile prestraining in the rolling direction (RD), followed by 2%, 5% or 10%

tensile straining in the 45° orientation and finally reloading in tension along the RD. The monotonic stress-strain curve in RD is also plotted.

4.3. Single SPCs of DP780 steel

Finally, the model is used to simulate the behavior of a DP780 steel after single SPCs. In the same manner as for the EDDQ steel, Ha et al. (2013) presented results from uniaxial tensile tests at every 15° from rolling direction after prestraining to 4% and 10% in uniaxial tension along the rolling direction. Fig. 8 shows the experimental and simulated reloading curves after the single SPC. Contrary to the EDDQ steel, this material does not exhibit stress overshooting. Instead, the reloading yield stress of the DP780 steel is below the monotonic loading curve in the same orientation and decreases with the angle of the second loading path. The decrease of the reloading yield stress is nearly the same for the two levels of prestrain. It also transpires that the proposed constitutive model is capable of describing the SPC behavior of the DP780 steel with good accuracy.

5. Discussion

The new yield function adopted in the proposed model is based on similar mathematics as the HAH model (Barlat et al., 2014), but the fluctuating part of the yield function is applied differently, namely to describe a distortional post-expansion of the yield surface in directions that are orthogonal to the microstructure deviator. A similar behavior of the yield surface is obtained in the HAH model based on splitting the deviatoric stress tensor into parts that are collinear and orthogonal to the direction of the microstructure deviator. In the HAH model, the yield surface is pre-distorted in the reversal part of the loading direction to capture reversal transients, while in the proposed model, the Bauschinger effect and hardening stagnation in reverse loading are described by combined isotropic and kinematic hardening rules, similar as by Mánik et al. (2015).

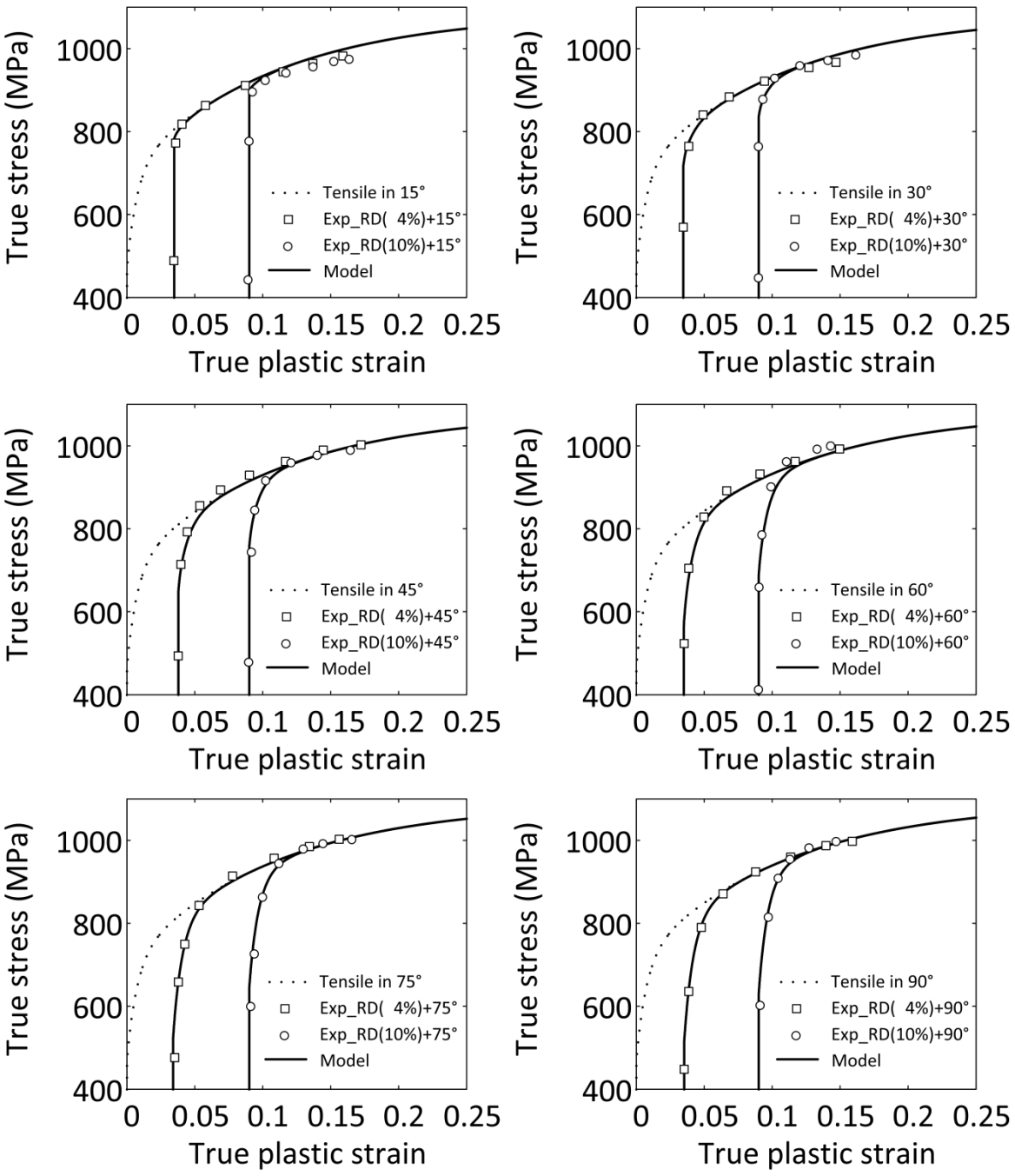

Fig. 8. DP780 steel: Experimental and simulated reloading curves in tension at every 15° after 4% and 10% prestrain in tension along the rolling direction (RD), together with the monotonic loading curve in the reloading direction.

Due to the kinematic hardening, the yield surface translates along the loading direction under monotonic loading, which leads to reduced yield stress not only in reverse, but also in orthogonal SPCs. In addition, an orthogonal SPC leads to an immediate distortional post-expansion of the yield surface along its orthogonal directions, as controlled by the internal variable S_o. Thus, by combining nonlinear kinematic hardening with orthogonal distortion of the yield surface, both the Bauschinger and cross-hardening effects are modeled. Hardening stagnation after a reverse SPC is captured by a transient isotropic expansion of the yield surface, as governed by the internal variable S_r.

The constitutive model relies on the microstructure deviator, $\hat{\mathbf{P}}$, which is a second order tensor. The direction of $\hat{\mathbf{P}}$ in the deviatoric stress space is interpreted as a memory of the microstructure directionality, and its magnitude mimics the amount of this microstructure. The angle between the microstructural deviator and the overstress tensor defines a Schmitt angle. For Schmitt angles lower than 90°, the microstructure will gradually change during plastic straining as a function of the current deviatoric stress state, by that $\hat{\mathbf{P}}$ is heading directly towards the new deviatoric stress direction. However, for Schmitt angles higher than 90°, the SPC is partly reversal, and reversible parts of the microstructure will first be destroyed before or simultaneously as the microstructure of the new strain path is built up (Barlat et al., 2003b). In the model, this reversal part is accounted for by that the evolution of the microstructure deviator tensor $\hat{\mathbf{P}}$ after such a SPC is first heading partly towards the origin. This is controlled by how the parameter k_p depends on the Schmitt angle, i.e., being smaller for Schmitt angles higher than 90°. Both the magnitude of the attractor $k_p\hat{\mathbf{N}}$ and the strain scale of the transient $k_p\Delta\varepsilon_P$ are influenced, so that immediately after a SPC with a Schmitt angle higher than 90°, the microstructure deviator tensor $\hat{\mathbf{P}}$ is shrinking faster and heading more towards the origin with increasing Schmitt angles.

The evolution of the yield surface and the microstructure deviator $\hat{\mathbf{P}}$ for EDDQ steel during uniaxial tensile loading along the y axis (90° direction) after 9.4% tensile prestrain along the x axis (rolling direction) is shown in Fig. 9. As kinematic hardening was neglected for this material, the yield surface expands isotopically during the preloading, as seen in Fig. 9a. Simultaneously, the microstructure deviator grows towards the deviatoric stress direction, as

illustrated in Fig. 9b. Each arrow corresponds to a specific equivalent plastic strain. The arrow at a plastic strain of 0.05 is shifted slightly from the origin, so that it can be distinguished in the figure. The stress-based Schmitt angle of this SPC is 120°. Subsequent to the SPC, the yield surface immediately expands rapidly in all directions orthogonal to the microstructure deviator $\hat{\mathbf{P}}$. Since $\hat{\mathbf{P}}$ now rotates gradually towards the new strain path, the distortionally expanded part of the yield surface rotates along with it. However, the yield surface reaches its maximum distortional expansion at the very early part of this rotation. During continued rotation, the expanded part of the yield surface vanishes gradually as the microstructure deviator becomes more and more collinear with the current deviatoric stress tensor.

Since the considered Schmitt angle in Fig. 9 is larger than 90°, the microstructure deviator is first heading partly towards the origin, i.e., it rapidly decreases and rotates to an intermediate state, which represents the partial annihilation of the microstructure created in the course of the preloading. Subsequently, when $\hat{\mathbf{P}}$ has rotated so that it points 90° to the new deviatoric stress direction, it grows and rotates, heading directly towards this direction, as can be seen in Fig. 9b. As it is approaching the new deviatoric stress direction, the orthogonal distortional hardening of the yield surface fades out, and the reloading curve approaches asymptotically the monotonic loading curve.

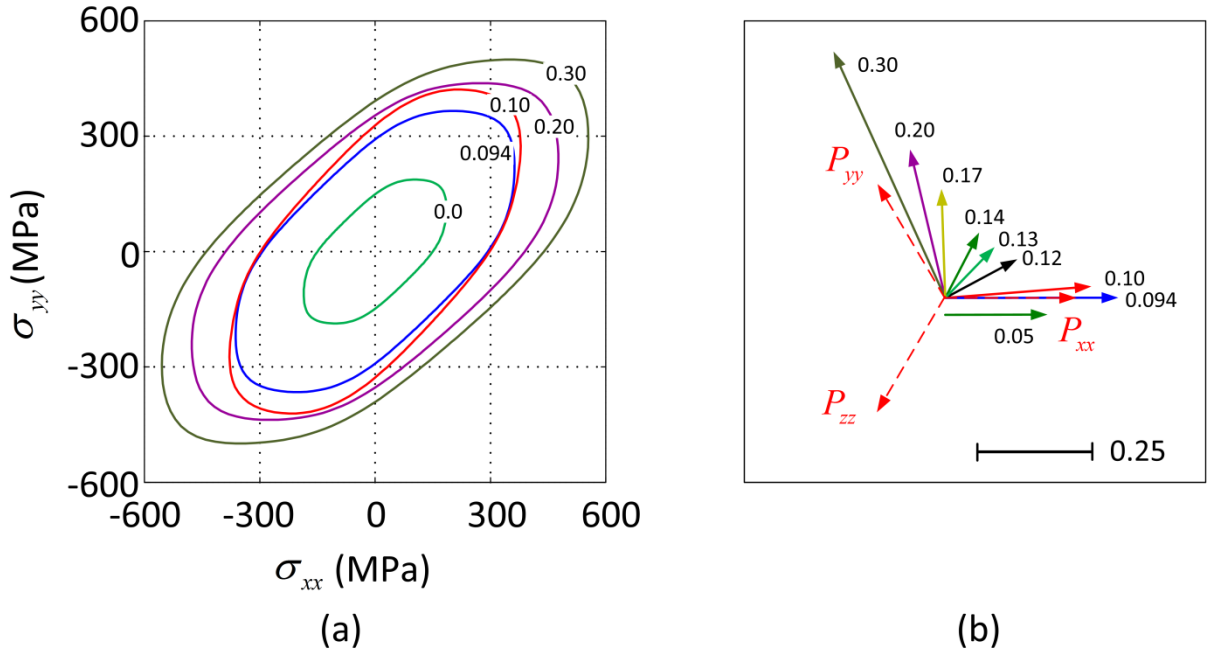

Fig. 9. Evolution of (a) the yield surface and (b) the microstructure deviator during loading in uniaxial tension along the y axis subsequent to 9.4% prestrain in uniaxial tension along the x axis. The numbers indicate the equivalent plastic strain levels.

The distortional post-expansion of the yield surface after an orthogonal SPC is important for the description of the double SPC presented in Section 4.2. Recall that the double SPC consisted of firstly 6% prestraining in tension along the rolling direction, secondly either 2%, 5% or 10% tensile straining in the 45° direction (corresponding to a stress-based Schmitt angle of 75.6°), and lastly reloading in tension along the rolling direction. The simulated results were shown in Fig. 7. As kinematic hardening is neglected for the EDDQ steel, the yield surface expands isotropically during preloading in the rolling direction, followed by distortional post-expansion along the orthogonal directions after the first change of the loading path, i.e., from tension along the rolling direction to tension along the 45° direction. Accordingly, a transient stress overshoot occurs during the second strain path. When the second SPC, i.e., back to the first strain path, occurs at the intermediate stage of the transient after the first SPC, a small stress overshoot is predicted subsequent to the last SPC, as compared with the monotonic loading curve without the SPCs, see Fig. 7. The microstructure deviator has in this case rotated into a new direction between the first and the second strain path directions. As evident from Fig. 7, a significant stress overshoot is obtained when the second SPC takes place during the final stage of the transient after the first

SPC. In such cases, the direction of the microstrucure deviator has had time to almost reach the second loading path. This behaviour is similar as predicted by the simpler models with isotropic post-expansion of the yield surface (Barlat et al., 2013; Mánik et al., 2015). However, when the second SPC occurs early in this transient, the final reloading curve nearly coalesces with the monotonic loading curve of the first strain path, see Fig. 7. This is reasonble, because there will have been limited time for changes of the microstructure to occur during the limited straining in the 45° tensile direction during the second SPC. However, models with isotropic post-expansion of the yield surface (Barlat et al., 2013; Mánik et al., 2015) will predict a sudden expansion that is similar for all directions; hence, after returning to the first strain path, the yield surface will have to shrink rapidly and isotropically from this level, as explained in Qin et al. (2017). Double SPCs occur in complex forming operations and such apparent softening behavior could wrongly lead to predictions of flow instabilities by these models, while it is accounted for by the distortional post-expansion in the proposed model.

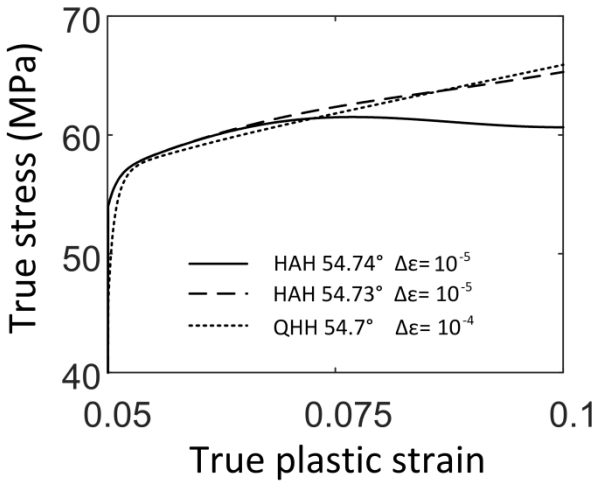

Fig. 10. Simulated reloading curves for AA1050 with tensile axis just below and just above 54.736° to RD after 5% prestrain along RD, i.e., nearly orthogonal SPCs. Note that the stable strain increment $\Delta\varepsilon$ is 10 times larger for the QHH model.

The QHH and the enhanced HAH models are quite similar in terms of what they can predict, and their calculation times should be about the same, depending on the time integration scheme used. The main difference is the way they model the Bauschinger effect, and differences may be expected for loading sequences in which orthogonal and reversal model terms play together. Hence, an orthogonal hardening simulation was conducted with both models for a material exhibiting a considerable Bauschinger effect, namely the AA1050 alloy. The parameters of the enhanced HAH model are again taken from Qin et al. (2017). The considered load sequence consists of 5% prestraining in tension along RD followed by tensile reloading at 54.736° to RD, corresponding to an orthogonal SPC. The results are shown in Fig. 10. In this case, a considerably smaller strain increment was required in the numerical integration of the enhanced HAH model than for the QHH model to get a stable and accurate solution. More importantly, it was found that the enhanced HAH model predicts two distinctly different reloading curves when approaching the limit of an orthogonal SPC from either a lower or higher Schmitt angle than 90°. In contrast, the QHH model provides similar curves and thus the behavior changes continuosly as the Schmitt angle goes through 90°. The origin of this spurious behavior is found in the original HAH model (Barlat et al., 2011), where the rotation direction of the microstructural deviator $\bar{\mathbf{h}}$ is opposite for Schmitt angles above and below 90°. If the Bauschinger effect is considerable, this behavior is unavoidable when the orthogonal and reversal model terms are

both active with similar strain scales. This was not observed by Barlat et al. (2014) for EDDQ steel because the expansion of the compressed part of the yield surface was very fast for this particular material.

In the current parameter identification process, all the experimental data are used to calibrate the model. The model is able to reproduce the available experimental data, but at present we cannot evaluate its predictive capabilities for other materials and more complex SPCs. Development of robust and standardized calibration procedures is important for future applications of advanced plasticity models like the one proposed here. However, like in similar earlier works (Haddadi et al., 2006; Barlat et al., 2014; Mánik et al., 2015), the main goal in this paper is to show the capability of the model rather than to develop a robust calibration procedure. An outline of such a procedure is given, but manual fine tuning is still required.

6. Conclusions

A new anisotropic hardening model has been developed, which describes monotonic loading and reverse SPC effects by combined nonlinear isotropic and kinematic hardening. The model is a generalization of the model by Mánik et al. (2015), introducing distortional post-expansion of the yield surface to handle complex, transient orthogonal SPC effects. A new formulation for orthogonal distortions has been proposed. Subsequent to orthogonal SPCs, the yield surface expands distortionally along directions being orthogonal to the direction of the microstructure deviator. After SPCs with Schmitt angles above 90°, the existing microstructure is assumed to partially dissolve before a new microstructure is formed, modeled by that the microstructure deviator first decreases in magnitude before heading in the direction of the current deviatoric overstress tensor. The model was assessed by simulating existing experimental tests for commercially pure aluminum, EDDQ and DP780 steels. It was found that the model is capable of describing the Bauschinger effect after general SPCs due to the back stress, the hardening stagnation and permanent softening after reverse SPCs, and transient hardening and permanent softening after orthogonal SPCs. The spurious behavior observed for nearly orthogonal SPCs with the enhanced HAH model is avoided with the QHH model.

Funding:

This research did not receive any specific grant from funding agencies in the public, commercial, or not-for-profit sectors.

References

Armstrong, P.J., Frederick, C.O., 1966. A mathematical representation of the multiaxial Bauschinger effect. A Mathematical Representation of the Multiaxial Bauschinger Effect. GEGB Report RD/B/N731.

Barlat, F., Brem, J.C., Yoon, J.W., Chung, K., Dick, R.E., Lege, D.J., Pourboghrat, F., Choi, S.H., Chu, E., 2003a. Plane stress yield function for aluminum alloy sheets—part 1: theory. Int. J. Plast. 19, 1297–1319.

Barlat, F., Duarte, J.M.F., Gracio, J.J., Lopes, A.B., Rauch, E.F., 2003b. Plastic flow for non-monotonic loading conditions of an aluminum alloy sheet sample. Int. J. Plast. 19, 1215–1244.

Barlat, F., Gracio, J.J., Lee, M.-G., Rauch, E.F., Vincze, G., 2011. An alternative to kinematic hardening in classical plasticity. Int. J. Plast. 27, 1309–1327.

Barlat, F., Ha, J., Grácio, J.J., Lee, M.-G., Rauch, E.F., Vincze, G., 2013. Extension of homogeneous anisotropic hardening model to cross-loading with latent effects. Int. J. Plast. 46, 130–142.

Barlat, F., Vincze, G., Grácio, J.J., Lee, M.-G., Rauch, E.F., Tomé, C.N., 2014. Enhancements of homogenous anisotropic hardening model and application to mild and dual-phase steels. Int. J. Plast. 58, 201–218.

Bauschinger, J., 1881. Changes of the elastic limit and the modulus of elasticity on various metals. Zivilingenieur 27, 289–348.

Belytschko, T., Liu, W.K., Moran, B., Elkhodary, K., 2013. Nonlinear finite elements for continua and structures. John wiley & sons.

Boers, S.H.A., Schreurs, P.J.G., Geers, M.G.D., Levkovitch, V., Wang, J., Svendsen, B., 2010. Experimental characterization and model identification of directional hardening effects in metals for complex strain path changes. Int. J. Solids Struct. 47, 1361–1374.

Boogaard, A.H., Riel, M., 2009. Non-proportional deformation paths for sheet metal: experiments and models. Form. Technol. Forum, ETH Zurich, Switzerland.

Bouvier, S., Alves, J.L., Oliveira, M.C., Menezes, L.F., 2005. Modelling of anisotropic work-hardening behaviour of metallic materials subjected to strain-path changes. Comput. Mater. Sci. 32, 301–315.

Cao, J., Yao, H., Karafillis, A., Boyce, M.C., 2000. Prediction of localized thinning in sheet metal using a general anisotropic yield criterion. Int. J. Plast. 16, 1105–1129.

Choi, Y., Han, C.-S., Lee, J.K., Wagoner, R.H., 2006. Modeling multi-axial deformation of planar anisotropic elasto-plastic materials, part I: Theory. Int. J. Plast. 22, 1745–1764.

Clausmeyer, T., Noman, M., Svendsen, B., 2009. Comparison of two models for anisotropic hardening evolution in metals during complex loading. Int. J. Mater. Form. 2, 395–398.

Feigenbaum, H.P., Dafalias, Y.F., 2007. Directional distortional hardening in metal plasticity within thermodynamics. Int. J. Solids Struct. 44, 7526–7542.

Ha, J., Lee, M.-G., Barlat, F., 2013. Strain hardening response and modeling of EDDQ and DP780 steel sheet under non-linear strain path. Mech. Mater. 64, 11–26.

Haddadi, H., Bouvier, S., Banu, M., Maier, C., Teodosiu, C., 2006. Towards an accurate description of the anisotropic behaviour of sheet metals under large plastic deformations: modelling, numerical analysis and identification. Int. J. Plast. 22, 2226–2271.

Hasegawa, T., Yakou, T., Karashima, S., 1975. Deformation behaviour and dislocation structures upon stress reversal in polycrystalline aluminium. Mater. Sci. Eng. 20, 267–276.

He, W.J., Zhang, S.H., Song, H.W., 2013. An extended homogenous yield function based anisotropic hardening model for description of anisotropic hardening behavior of materials. Int. J. Mech. Sci. 77, 343–355.

Hershey, A. V, 1954. The plasticity of an isotropic aggregate of anisotropic face-centered cubic crystals. J. Appl. Mech. Asme 21, 241–249.

Holmedal, B., Van Houtte, P., An, Y., 2008. A crystal plasticity model for strain-path changes in metals. Int. J. Plast. 24, 1360–1379.

Keeler, S.P., Backofen, W.A., 1963. Plastic instability and fracture in sheets stretched over rigid punches. Asm Trans Q 56, 25–48.

Khan, A.S., Huang, S., 1995. Continuum theory of plasticity. A Wiley Inerscience Publ. John Wiley Sons, Inc. USA 421.

Kitayama, K., Tomé, C.N., Rauch, E.F., Gracio, J.J., Barlat, F., 2013. A crystallographic dislocation model for describing hardening of polycrystals during strain path changes. Application to low carbon steels. Int. J. Plast. 46, 54–69.

Lee, J.-W., Lee, M.-G., Barlat, F., 2012. Finite element modeling using homogeneous anisotropic hardening and application to spring-back prediction. Int. J. Plast. 29, 13–41.

Levkovitch, V., Svendsen, B., 2007. Accurate hardening modeling as basis for the realistic simulation of sheet forming processes with complex strain-path changes, in: 10th ESAFORM Conference on Material Forming. AIP Publishing, pp. 358–363.

Li, F., Bate, P.S., 1991. Strain path change effects in cube textured aluminium sheet. Acta Metall. Mater. 39, 2639–2650.

Mánik, T., Holmedal, B., Hopperstad, O.S., 2015. Strain-path change induced transients in flow stress, work hardening and r-values in aluminum. Int. J. Plast. 69, 1–20.

Manopulo, N., Barlat, F., Hora, P., 2015. Isotropic to distortional hardening transition in metal plasticity. Int. J. Solids Struct. 56, 11–19.

Orowan, E., Rassweiler, G.M., Grube, W.L., 1959. Internal Stresses and Fatigue in Metals, in: Causes and Effects of Internal Stresses. New York: Elsevier., pp. 59–80.

Peeters, B., Bacroix, B., Teodosiu, C., Van Houtte, P., Aernoudt, E., 2001a. Work-hardening/softening behaviour of bcc polycrystals during changing strain:: Part II. TEM observations of dislocation sheets in an IF steel during two-stage strain paths and their representation in terms of dislocation densities. Acta Mater. 49, 1621–1632.

Peeters, B., Seefeldt, M., Teodosiu, C., Kalidindi, S.R., Van Houtte, P., Aernoudt, E., 2001b. Work-hardening/softening behaviour of b.c.c. polycrystals during changing strain paths: I. An integrated model based on substructure and texture evolution, and its prediction of the stress–strain behaviour of an IF steel during two-stage strain paths. Acta Mater. 49, 1607–1619.

Qin, J., Holmedal, B., Zhang, K., Hopperstad, O.S., 2017. Modeling strain-path changes in aluminum and steel. Int. J. Solids Struct. 117, 123–136.

Rockafellar, R.T., 1970. Convex Analysis (Princeton Mathematical Series). Princet. Univ. Press.

Schmitt, J.H., Shen, E.L., Raphanel, J.L., 1994. A parameter for measuring the magnitude of a change of strain path: Validation and comparison with experiments on low carbon steel. Int. J. Plast. 10, 535–551.

Teodosiu, C., Hu, Z., 1995. Evolution of the intragranular microstructure at moderate and large strains: modelling and computational significance, in: Proc. Numiform. pp. 173–182.

Vincze, G., Barlat, F., Rauch, E.F., Tomé, C.N., Butuc, M.C., Grácio, J.J., 2013. Experiments and modeling of low carbon steel sheet subjected to double strain path changes. Metall. Mater. Trans. A 44, 4475–4479.

Voce, E., 1948. The relationship between stress and strain for homogeneous deformation. J Inst Met 74, 537–562.

Wang, J., Levkovitch, V., Reusch, F., Svendsen, B., Huetink, J., Van Riel, M., 2008. On the modeling of hardening in metals during non-proportional loading. Int. J. Plast. 24, 1039–1070.

Wang, J., Levkovitch, V., Svendsen, B., 2006. Modeling and simulation of directional hardening in metals during non-proportional loading. J. Mater. Process. Technol. 177, 430–432.

Wen, W., Borodachenkova, M., Tomé, C.N., Vincze, G., Rauch, E.F., Barlat, F., Grácio, J.J., 2016. Mechanical behavior of low carbon steel subjected to strain path changes: Experiments and modeling. Acta Mater. 111, 305–314.

Wen, W., Borodachenkova, M., Tomé, C.N., Vincze, G., Rauch, E.F., Barlat, F., Grácio, J.J., 2015. Mechanical behavior of Mg subjected to strain path changes: Experiments and modeling. Int. J. Plast. 73, 171–183.

Yao, H., Cao, J., 2002. Prediction of forming limit curves using an anisotropic yield function with prestrain induced backstress. Int. J. Plast. 18, 1013–1038.

Yoshida, F., Hamasaki, H., Uemori, T., 2015. Modeling of anisotropic hardening of sheet metals including description of the Bauschinger effect. Int. J. Plast. 75, 170–188.